PHYSICAL REVIEW A **102**, 033727 (2020)

Enantiomeric-excess determination based on nonreciprocal-transition-induced spectral-line elimination

Xun-Wei Xu,[1,2,*] Chong Ye,[3,4] Yong Li,[4,1,†] and Ai-Xi Chen[5,2,‡]

[1] *Key Laboratory of Low-Dimensional Quantum Structures and Quantum Control of Ministry of Education, Department of Physics and Synergetic Innovation Center for Quantum Effects and Applications, Hunan Normal University, Changsha 410081, China*
[2] *Department of Applied Physics, East China Jiaotong University, Nanchang 330013, China*
[3] *Beijing Key Laboratory of Nanophotonics and Ultrafine Optoelectronic Systems, School of Physics, Beijing Institute of Technology, Beijing 100081, China*
[4] *Beijing Computational Science Research Center, Beijing 100193, China*
[5] *Department of Physics, Zhejiang Sci-Tech University, Hangzhou 310018, China*

(Received 19 February 2020; accepted 9 September 2020; published 28 September 2020)

The spontaneous emission spectrum of a multilevel atom or molecule with nonreciprocal transition is investigated. It is shown that the nonreciprocal transition can lead to the elimination of a spectral line in the spontaneous emission spectrum. As an application, we show that nonreciprocal transition arises from the phase-related driving fields in chiral molecules with cyclic three-level transitions, and the elimination of a spectral line induced by nonreciprocal transition provides us a method to determine the enantiomeric excess for the chiral molecules without requiring the enantio-pure samples.

DOI: 10.1103/PhysRevA.102.033727

I. INTRODUCTION

Nonreciprocity is a very general concept that arises in many branches of physics, such as electronics, optics [1,2], acoustics [3,4], and condensed-matter physics [5]. Nonreciprocity means that some particles or waves exhibit different transmission properties when their sources and detectors are exchanged, such as the one-way electric conduction in the semiconductor p-n junctions. In a recent paper [6], some of us introduced the concept of nonreciprocity to investigate the transitions between different energy levels, and proposed a generic method to realize significant difference between the stimulated emission and absorption coefficients of two nondegenerate energy levels, which we refer to as nonreciprocal transition [6]. The nonreciprocal transition can be used for many applications, such as single-photon nonreciprocal transporter [6], nonreciprocal phonon devices [7,8], and the echo cancellation in quantum memory [9] and quantum measurements [10].

In this paper, we will study the spontaneous emission of a multilevel atom or molecule with nonreciprocal transition. The spontaneous emission spectrum emitted from an atom or molecule shows a valuable insight into the behavior of transitions between different energy levels [11,12]. We find that the nonreciprocal transition can be reflected with spectral-line elimination in the spontaneous emission spectra, which provides us a very simple way to test nonreciprocal transition in experiment.

On the other hand, chirality is important in chemistry and biology for many chemical and biological processes are chirality dependent [13]. But the chiral discrimination and separation remain challenging works under the existing experimental technical conditions. Some spectroscopic methods have been developed to determine enantiomeric excess, such as circular dichroism [14,15], Raman optical activity [16,17], and spectroscopy for a cyclic three-level model [18–20] based on quantum interference effects [21], three-wave mixing [22–33], ac Stark effect [34], or deflection effect [35]. In addition, many methods were proposed to achieve inner-state separating [36–43] or spatially separating [44–49] molecules of different chiralities, and enantioconversion of chiral mixtures [50–55].

In the latter part of this paper, we apply the general theory of the spontaneous emission of multilevel systems to the chiral molecules. We show that nonreciprocal transition arises from the phase-related driving fields for chiral molecules with cyclic three-level transitions and the appearance of spectral-line elimination in the spontaneous emission spectra around some resonant frequencies is chirality dependent. Therefore, the enantiomeric excess can be determined by measuring the spontaneous emission spectra of chiral molecules. Different from the traditional methods of enantiomeric-excess determination [14–16], the spectral-line elimination in the spontaneous emission spectrum induced by nonreciprocal transition provides us another method to determine the enantiomeric excess for chiral molecules without requiring the enantio-pure samples. Our work also strongly differs from the previous study by Eibenberger *et al.* [30], who proposed a dynamic method to create state-selective enantiomeric excess of chiral molecules with the transitions driven by a sequence of microwave pulses. In the dynamic method the lengths

---

[*] davidxu0816@163.com
[†] liyong@csrc.ac.cn
[‡] aixichen@zstu.edu.cn

©2020 American Physical Society

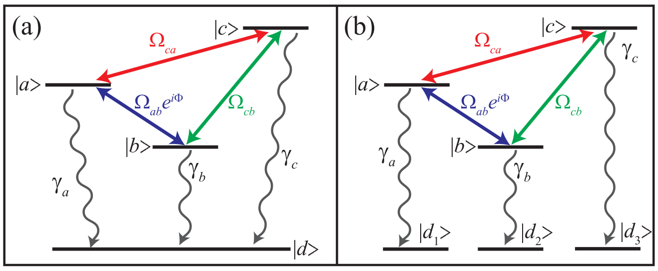

FIG. 1. Level diagram of an atom or molecule with cyclic transitions for the three upper levels ($|a\rangle$, $|b\rangle$, and $|c\rangle$), and they are coupled by the same vacuum modes to (a) the common lower level ($|d\rangle$) or (b) different lower levels ($|d_1\rangle$, $|d_2\rangle$, and $|d_3\rangle$).

and intensities of the pulses should be chosen properly for enantiomer-specific state transfer, whereas in our work, the transitions are driven by continuous-wave lasers with constant intensities and the spontaneous emission spectra are measured after a long period of stability, which give rise to markedly different behaviors.

The remainder of this paper is organized as follows. In Sec. II, the basic theory for spontaneous emission spectrum of a general multilevel system with nonreciprocal transition is introduced. The time evolution of the populations and the corresponding spontaneous emission spectra of the multilevel system with nonreciprocal transition are investigated in detail in Sec. III. The application of the spontaneous emission spectra in determining the enantiomeric excess for chiral molecules are discussed in Sec. IV. Finally, a summary is given in Sec. V.

II. BASIC THEORY FOR SPONTANEOUS EMISSION SPECTRUM

We study the spontaneous emission of an atom or molecule with three upper levels ($|a\rangle$, $|b\rangle$, and $|c\rangle$), which are coupled to each other by three strong fields with frequencies (ν_{ab}, ν_{cb}, and ν_{ca}), Rabi frequencies (Ω_{ab}, Ω_{cb}, and Ω_{ca}), and phases (ϕ_{ab}, ϕ_{cb}, and ϕ_{ca}). The spontaneous emission spectrum for the system will be derived for two different cases: (A) the three upper levels are coupled to one common lower level ($|d\rangle$) with the same vacuum modes, as shown in Fig. 1(a), or (B) the three upper levels are coupled to three different lower levels ($|d_1\rangle$, $|d_2\rangle$, and $|d_3\rangle$), respectively, with the same vacuum modes, as shown in Fig. 1(b).

A. With one common lower level

Consider the three upper levels ($|a\rangle$, $|b\rangle$, and $|c\rangle$) coupled with one common lower level ($|d\rangle$) by the same vacuum modes. The interaction Hamiltonian of the system in the interaction picture can be written as ($\hbar = 1$)

$$\begin{aligned} V = {} & \Omega_{ab}e^{i\Phi}e^{i\Delta_{ab}t}|a\rangle\langle b| + \Omega_{cb}e^{i\Delta_{cb}t}|c\rangle\langle b| + \Omega_{ca}e^{i\Delta_{ca}t}|c\rangle\langle a| \\ & + \sum_k \left[g_k^{ad}e^{i(\omega_{ad}-\omega_k)t}v_k|a\rangle\langle d| + g_k^{bd}e^{i(\omega_{bd}-\omega_k)t}v_k|b\rangle\langle d| + g_k^{cd}e^{i(\omega_{cd}-\omega_k)t}v_k|c\rangle\langle d|\right] + \text{H.c.}, \end{aligned} \tag{1}$$

where $\omega_{\sigma\sigma'}$ ($\sigma, \sigma' = a, b, c, d$) are the frequency differences between levels $|\sigma\rangle$ and $|\sigma'\rangle$, $\Delta_{\sigma\sigma'} = \omega_{\sigma\sigma'} - \nu_{\sigma\sigma'}$ is the detuning of the driving fields, v_k ($v_k^\dagger$) is the annihilation (creation) operator for the kth vacuum mode with frequency ω_k, and $g_k^{\sigma d}$ is the coupling constant between the kth vacuum mode and the atomic transition from $|\sigma\rangle$ to $|d\rangle$. Here k denotes both the momentum and polarization of the vacuum modes, and the total phase $\Phi = \phi_{ab} - \phi_{cb} + \phi_{ca}$ is obtained by redefining $e^{-i\phi_{cb}}|b\rangle \rightarrow |b\rangle$ and $e^{-i\phi_{ca}}|a\rangle \rightarrow |a\rangle$. As the phase of the coupling constant $g_k^{\sigma d}$ does not matter in the following discussions, real $g_k^{\sigma d}$ is assumed for notational convenience.

We assume the system is initially prepared in one of the upper levels, i.e., $|\psi(0)\rangle = |b\rangle|0\rangle$, where $|0\rangle$ denotes the vacuum state. The state vector at time t can be written as

$$|\psi(t)\rangle = \left[A(t)|a\rangle + B(t)|b\rangle + C(t)|c\rangle + \sum_k D_k(t)v_k^\dagger|d\rangle\right]|0\rangle, \tag{2}$$

where the modulus squares of the coefficients $A(t)$, $B(t)$, $C(t)$, and $D_k(t)$ are the occupation probabilities in the corresponding state at time t. By using the Weisskopf-Wigner approximation [56,57], the dynamical behaviors for the coefficients are given by

$$\begin{aligned} \frac{d}{dt}A(t) = {} & -\frac{\gamma_a}{2}A(t) - p_{ab}\frac{\sqrt{\gamma_a\gamma_b}}{2}e^{i\omega_{ab}t}B(t) - p_{ca}\frac{\sqrt{\gamma_a\gamma_c}}{2}e^{-i\omega_{ca}t}C(t) \\ & - i\Omega_{ab}e^{i\Phi}e^{i\Delta_{ab}t}B(t) - i\Omega_{ca}e^{-i\Delta_{ca}t}C(t), \end{aligned} \tag{3}$$

$$\begin{aligned} \frac{d}{dt}B(t) = {} & -\frac{\gamma_b}{2}B(t) - p_{ab}\frac{\sqrt{\gamma_a\gamma_b}}{2}e^{-i\omega_{ab}t}A(t) - p_{cb}\frac{\sqrt{\gamma_b\gamma_c}}{2}e^{-i\omega_{cb}t}C(t) \\ & - i\Omega_{cb}e^{-i\Delta_{cb}t}C(t) - i\Omega_{ab}e^{-i\Phi}e^{-i\Delta_{ab}t}A(t), \end{aligned} \tag{4}$$

$$\begin{aligned} \frac{d}{dt}C(t) = {} & -\frac{\gamma_c}{2}C(t) - p_{ca}\frac{\sqrt{\gamma_a\gamma_c}}{2}e^{i\omega_{ca}t}A(t) - p_{cb}\frac{\sqrt{\gamma_c\gamma_b}}{2}e^{i\omega_{cb}t}B(t) \\ & - i\Omega_{ca}e^{i\Delta_{ca}t}A(t) - i\Omega_{cb}e^{i\Delta_{cb}t}B(t), \end{aligned} \tag{5}$$

$$\frac{d}{dt}D_k(t) = -ig_k^{ad}e^{-i(\omega_{ad}-\omega_k)t}A(t) - ig_k^{bd}e^{-i(\omega_{bd}-\omega_k)t}B(t) - ig_k^{cd}e^{-i(\omega_{cd}-\omega_k)t}C(t), \tag{6}$$

where $\gamma_a = [2\pi(g_k^{ad})^2\rho(\omega_k)]_{\omega_k=\omega_{ad}}$, $\gamma_b = [2\pi(g_k^{bd})^2\rho(\omega_k)]_{\omega_k=\omega_{bd}}$, and $\gamma_c = [2\pi(g_k^{cd})^2\rho(\omega_k)]_{\omega_k=\omega_{cd}}$ are the decay rates, $\rho(\omega_k)$ is the mode density, $p_{\sigma\sigma'} = \vec{\mu}_\sigma \cdot \vec{\mu}_{\sigma'}/(|\vec{\mu}_\sigma| \cdot |\vec{\mu}_{\sigma'}|)$, and $\vec{\mu}_\sigma$ ($\vec{\mu}_{\sigma'}$) is the dipole moment of the transition from $|\sigma\rangle$ ($|\sigma'\rangle$) to $|d\rangle$ ($\sigma, \sigma' = a, b, c$). The coupling terms with $p_{\sigma\sigma'}$ are induced by the decays from different upper levels ($|\sigma\rangle$ and $|\sigma'\rangle$) to the common lower level $|d\rangle$, which can result in spontaneous emission cancellation and spectral-line elimination [11,12]. However, here we have assumed $\min\{\omega_{ab}, \omega_{ca}, \omega_{cb}\} \gg \max\{\gamma_a, \gamma_b, \gamma_c, \Omega_{ab}, \Omega_{cb}, \Omega_{ca}, \Delta_{ab}, \Delta_{ca}, \Delta_{cb}\}$ so that the rapidly rotating terms (i.e., the decay induced coupling terms with $p_{\sigma\sigma'}\frac{\sqrt{\gamma_\sigma\gamma_{\sigma'}}}{2}e^{\pm i\omega_{\sigma\sigma'}t}$) in Eqs. (3)–(5) can be neglected, and the dynamical equations are simplified as

$$\frac{d}{dt}A(t) = -\frac{\gamma_a}{2}A(t) - i\Omega_{ab}e^{i\Phi}e^{i\Delta_{ab}t}B(t) - i\Omega_{ca}e^{-i\Delta_{ca}t}C(t), \tag{7}$$

$$\frac{d}{dt}B(t) = -\frac{\gamma_b}{2}B(t) - i\Omega_{cb}e^{-i\Delta_{cb}t}C(t) - i\Omega_{ab}e^{-i\Phi}e^{-i\Delta_{ab}t}A(t), \tag{8}$$

$$\frac{d}{dt}C(t) = -\frac{\gamma_c}{2}C(t) - i\Omega_{ca}e^{i\Delta_{ca}t}A(t) - i\Omega_{cb}e^{i\Delta_{cb}t}B(t). \tag{9}$$

For convenience of calculations, let us define $\widetilde{B}(t) \equiv e^{i\Delta_{ab}t}B(t)$ and $\widetilde{C}(t) \equiv e^{-i\Delta_{ca}t}C(t)$ and make the assumption of three-photon resonance $\Delta_{ca} + \Delta_{ab} = \Delta_{cb}$; then we get dynamical equations with constant coefficients as

$$\frac{dA(t)}{dt} = -\frac{\gamma_a}{2}A(t) - i\Omega_{ab}e^{i\Phi}\widetilde{B}(t) - i\Omega_{ca}\widetilde{C}(t), \tag{10}$$

$$\frac{d\widetilde{B}(t)}{dt} = -\left(\frac{\gamma_b}{2} - i\Delta_{ab}\right)\widetilde{B}(t) - i\Omega_{cb}\widetilde{C}(t) - i\Omega_{ab}e^{-i\Phi}A(t), \tag{11}$$

$$\frac{d\widetilde{C}(t)}{dt} = -\left(\frac{\gamma_c}{2} + i\Delta_{ca}\right)\widetilde{C}(t) - i\Omega_{ca}A(t) - i\Omega_{cb}\widetilde{B}(t). \tag{12}$$

All the following calculations and discussions on the occupation probabilities are based on Eqs. (10)–(12).

In the following, we will use the Laplace transform method to solve the dynamic equations. By taking the Laplace transform, i.e., $\overline{O}(s) = \int_0^{+\infty} O(t)e^{-st}dt$, of Eqs. (10)–(12), with the initial condition $\Psi_0 = [A(0), \widetilde{B}(0), \widetilde{C}(0)]^T$, we get [11,12]

$$\overline{\Psi} = M^{-1}\Psi_0, \tag{13}$$

with $\overline{\Psi} = [\overline{A}(s), \overline{\widetilde{B}}(s), \overline{\widetilde{C}}(s)]^T$, and

$$M = \begin{pmatrix} s + \frac{\gamma_a}{2} & i\Omega_{ab}e^{i\Phi} & i\Omega_{ca} \\ i\Omega_{ab}e^{-i\Phi} & s + \frac{\gamma_b}{2} - i\Delta_{ab} & i\Omega_{bc} \\ i\Omega_{ca} & i\Omega_{cb} & s + \frac{\gamma_c}{2} + i\Delta_{ca} \end{pmatrix}. \tag{14}$$

The spontaneous emission spectrum of the system [11,12], $S(\omega)$, is the Fourier transform of

$$\begin{aligned} \langle E^-(t+\tau)E^+(t)\rangle_{t\to+\infty} &\equiv \langle\psi(t)|\sum_{k,k'} v_k^\dagger e^{i\omega_k(t+\tau)}v_{k'}e^{-i\omega_{k'}t}|\psi(t)\rangle_{t\to+\infty} \\ &= \int_{-\infty}^{+\infty} |D_k(+\infty)|^2\rho(\omega_k)e^{i\omega_k\tau}d\omega_k. \end{aligned} \tag{15}$$

Then we have $S(\omega_k) = |D_k(+\infty)|^2\rho(\omega_k)$, where $D_k(+\infty)$ is the long-time behavior ($t \to +\infty$) of $D_k(t)$ and can be obtained by integrating time t' in Eq. (6) as

$$\begin{aligned} D_k(+\infty) &= \int_0^{+\infty} \left[-ig_k^{ad}e^{-i(\omega_{ad}-\omega_k)t'}A(t') - ig_k^{bd}e^{-i(\omega_{bd}-\omega_k+\Delta_{ab})t'}\widetilde{B}(t') - ig_k^{cd}e^{-i(\omega_{cd}-\omega_k-\Delta_{ca})t'}\widetilde{C}(t')\right]dt' \\ &= -ig_k^{ad}\overline{A}(-i\delta_k) - ig_k^{bd}\overline{\widetilde{B}}\big(-i\delta_k^b\big) - ig_k^{cd}\overline{\widetilde{C}}\big(-i\delta_k^c\big), \end{aligned} \tag{16}$$

with the detunings $\delta_k \equiv \omega_k - \omega_{ad}$, $\delta_k^b \equiv \delta_k + \omega_{ab} - \Delta_{ab}$, and $\delta_k^c \equiv \delta_k - \omega_{ca} + \Delta_{ca}$. Finally, the spontaneous emission spectrum is given by

$$S(\omega_k) = \frac{1}{2\pi}\left|\sqrt{\gamma_a}\overline{A}(-i\delta_k) + \sqrt{\gamma_b}\overline{\widetilde{B}}\big(-i\delta_k^b\big) + \sqrt{\gamma_c}\overline{\widetilde{C}}\big(-i\delta_k^c\big)\right|^2, \tag{17}$$

with $\overline{A}(s)$, $\overline{\widetilde{B}}(s)$, and $\overline{\widetilde{C}}(s)$ given by Eq. (13).

B. With three different lower levels

In the case with three different lower levels, the interaction Hamiltonian of the system is given in the interaction picture by

$$\begin{aligned} V' &= \Omega_{ab}e^{i\Phi}e^{i\Delta_{ab}t}|a\rangle\langle b| + \Omega_{cb}e^{i\Delta_{cb}t}|c\rangle\langle b| + \Omega_{ca}e^{i\Delta_{ca}t}|c\rangle\langle a| \\ &\quad + \sum_k \left[g_k^{ad_1}e^{i(\omega_{ad_1}-\omega_k)t}v_k|a\rangle\langle d_1| + g_k^{bd_2}e^{i(\omega_{bd_2}-\omega_k)t}v_k|b\rangle\langle d_2| + g_k^{cd_3}e^{i(\omega_{cd_3}-\omega_k)t}v_k|c\rangle\langle d_3|\right] + \text{H.c.}, \end{aligned} \tag{18}$$

where $\omega_{\sigma d_j}$ denote the frequency differences between levels $|\sigma\rangle$ ($\sigma = a, b, c$) and $|d_j\rangle$ ($j = 1, 2, 3$), and $g_k^{\sigma d_j}$ is the coupling constant between the kth vacuum mode and the atomic transition from $|\sigma\rangle$ to $|d_j\rangle$. The state vector for the system at time t can be written as

$$|\psi'(t)\rangle = \left[A(t)|a\rangle + B(t)|b\rangle + C(t)|c\rangle + \sum_{j=1,2,3}\sum_k D_{j,k}(t)v_k^\dagger|d_j\rangle\right]|0\rangle, \tag{19}$$

where the modulus square of the coefficient $D_{j,k}(t)$ is the occupation probability in the state $v_k^\dagger|d_j\rangle|0\rangle$ at time t.

By substituting the Hamiltonian and state vector into the Schrödinger equation and using the Weisskopf-Wigner approximation, the dynamic equations of the coefficients [$A(t)$, $B(t)$, and $C(t)$] are obtained and they have the same forms as those given by Eqs. (7)–(9), with the decay rates replaced by $\gamma_a' = [2\pi(g_k^{ad_1})^2\rho(\omega_k)]_{\omega_k=\omega_{ad_1}}$, $\gamma_b' = [2\pi(g_k^{bd_2})^2\rho(\omega_k)]_{\omega_k=\omega_{bd_2}}$, and $\gamma_c' = [2\pi(g_k^{cd_3})^2\rho(\omega_k)]_{\omega_k=\omega_{cd_3}}$. The spontaneous emission spectrum is obtained as $S(\omega_k) = \sum_{j=1,2,3}|D_{j,k}(+\infty)|^2\rho(\omega_k)$, where

$$D_{1,k}(+\infty) = -ig_k^{ad_1}\overline{A}(-i\delta_k'), \tag{20}$$

$$D_{2,k}(+\infty) = -ig_k^{bd_2}\overline{\overline{B}}(-i\delta_k^{b\prime}), \tag{21}$$

$$D_{3,k}(+\infty) = -ig_k^{cd_3}\widetilde{\overline{C}}(-i\delta_k^{c\prime}), \tag{22}$$

the coefficients [$\overline{A}(s)$, $\overline{\overline{B}}(s)$, and $\widetilde{\overline{C}}(s)$] are given by Eq. (13), and the detunings are defined by $\delta_k' \equiv \omega_k - \omega_{ad_1}$, $\delta_k^{b\prime} \equiv \omega_k - \omega_{bd_2} - \Delta_{ab} = \delta_k' + \omega_{ab}' - \Delta_{ab}$, and $\delta_k^{c\prime} \equiv \omega_k - \omega_{cd_3} + \Delta_{ca} = \delta_k' - \omega_{ca}' + \Delta_{ca}$, with $\omega_{ab}' \equiv \omega_{ad_1} - \omega_{bd_2}$ and $\omega_{ca}' \equiv \omega_{cd_3} - \omega_{ad_1}$. Thus the spontaneous emission spectrum for the case with three different lower levels can be specifically expressed as

$$S(\omega_k) = \frac{1}{2\pi}\left\{\gamma_a|\overline{A}(-i\delta_k')|^2 + \gamma_b\left|\overline{\overline{B}}(-i\delta_k^{b\prime})\right|^2 + \gamma_c\left|\widetilde{\overline{C}}(-i\delta_k^{c\prime})\right|^2\right\}. \tag{23}$$

For comparison with the case of one common lower level given by Eq. (17) in the following, we assume that $\omega_{ad_1} = \omega_{ad}$, $\omega_{bd_2} = \omega_{bd}$, and $\omega_{cd_3} = \omega_{cd}$, i.e., the three lower levels $|d_j\rangle$ ($j = 1, 2, 3$) are degenerate, so that we have $\delta_k' = \delta_k$, $\omega_{ab}' = \omega_{ab}$, $\omega_{ca}' = \omega_{ca}$, $\delta_k^{b\prime} = \delta_k^b$, $\delta_k^{c\prime} = \delta_k^c$, $\gamma_a' = \gamma_a$, $\gamma_b' = \gamma_b$, and $\gamma_c' = \gamma_c$. However, we should point out that this assumption does not bring significant differences in physical appearance except the positions of resonance peaks in the spectra.

III. NONRECIPROCAL TRANSITION AND THE SPONTANEOUS EMISSION SPECTRA

First, let us investigate the time evolution of the upper-level populations and the transition probabilities $T_{ab}(t)$ and $T_{ba}(t)$ between the upper levels $|a\rangle$ and $|b\rangle$. As the decay induced coupling terms with $p_{\sigma\sigma'}\frac{\sqrt{\gamma_\sigma\gamma_{\sigma'}}}{2}e^{\pm i\omega_{\sigma\sigma'}t}$ in Eqs. (3)–(5) are high-frequency oscillating terms and neglected safely under the assumption $\{\omega_{ab}, \omega_{ca}, \omega_{cb}\} \gg \{\gamma_a, \gamma_b, \gamma_c, \Delta_{ab}, \Delta_{ca}, \Delta_{cb}\}$, the time evolutions of the upper-level populations are the same for both the two cases with one common or three different lower levels.

The populations $|A(t)|^2$ (black solid curve) and $|B(t)|^2$ (red dashed curve) obtained from Eqs. (10)–(12) are plotted as functions of the time t in Figs. 2(a)–2(d). It is clear that the population can transfer from the level $|a\rangle$ to level $|b\rangle$ for $\Phi = \pi/2$, but almost no population will transfer from the level $|b\rangle$ to level $|a\rangle$. In contrast, the population can transfer from the level $|b\rangle$ to level $|a\rangle$, but almost no population will transfer from the level $|a\rangle$ to level $|b\rangle$ when $\Phi = 3\pi/2$.

The transition probabilities from $|b\rangle$ to $|a\rangle$ [$T_{ab}(t)$] and from $|a\rangle$ to $|b\rangle$ [$T_{ba}(t)$] can also be obtained from Eqs. (10)–(12); see the Appendix for details. They are plotted as functions of time t in Figs. 2(e) and 2(f). It is clear that $T_{ab}(t) \ll T_{ba}(t)$ for $\phi = \pi/2$ and $T_{ab}(t) \gg T_{ba}(t)$ for $\phi = 3\pi/2$, i.e., the transitions between levels $|b\rangle$ and $|a\rangle$ are nonreciprocal. As discussed in Ref. [6], there are two ingredients for nonreciprocal transitions in the system: One is the synthetic magnetic flux, i.e., the total phase Φ in the cyclic transition, which breaks the time-reversal symmetry of the system, and the other one is the decay rates of upper levels, which play a key role in suppressing the transition probabilities in one direction but not the other.

The nonreciprocal transitions can be observed by measuring the spontaneous emission spectra of the system. As an example, the system is prepared in level $|b\rangle$ initially. When $\Phi = 3\pi/2$, as the population can transfer from the level $|b\rangle$ to level $|a\rangle$, there should be a peak around the resonant frequency ω_{ad}. In contrast, if $\Phi = \pi/2$, almost no population can be transferred from the level $|b\rangle$ to level $|a\rangle$, so that the peak around the frequency ω_{ad} will be eliminated (i.e., a dip should appear there).

In Fig. 3, the spontaneous emission spectra of the system are plotted for the three upper levels ($|a\rangle$, $|b\rangle$, and $|c\rangle$) coupled by the same vacuum modes to (a) the common lower level

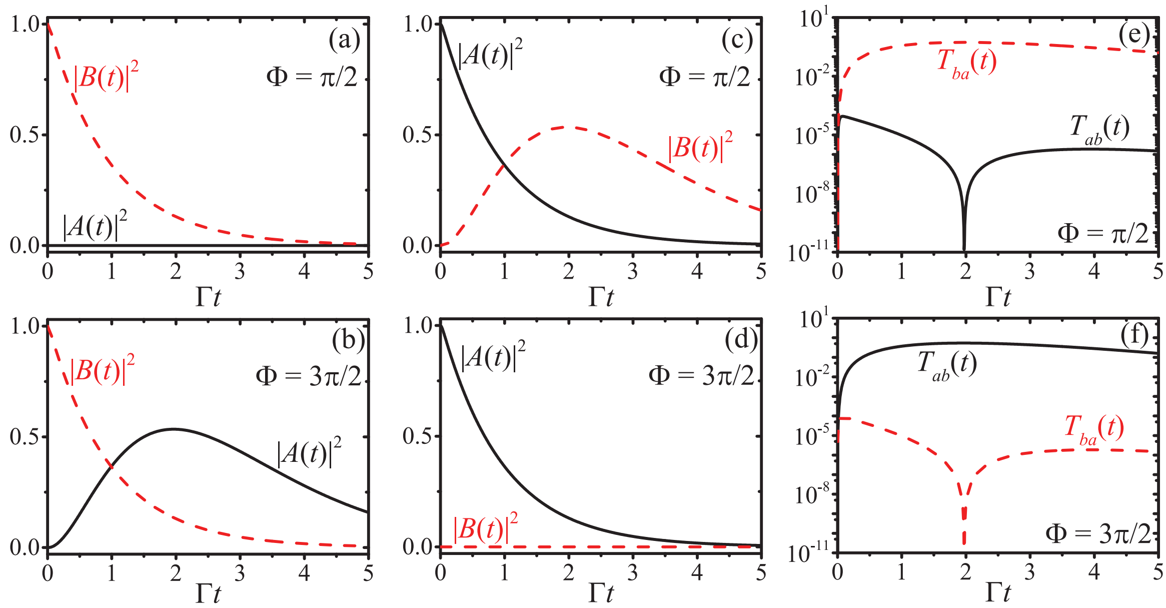

FIG. 2. Populations $|A(t)|^2$ (black solid curve) and $|B(t)|^2$ (red dashed curve) are plotted as functions of the time Γt for $\Phi = \pi/2$ in (a) and (c) and $\Phi = 3\pi/2$ in (b) and (d). The initial conditions are $A(0) = C(0) = 0$ and $B(0) = 1$ for (a) and (b) and $B(0) = C(0) = 0$ and $A(0) = 1$ for (c) and (d). The transition probabilities $T_{ab}(t)$ and $T_{ba}(t)$ are plotted as functions of the time Γt for (e) $\Phi = \pi/2$ and (f) $\Phi = 3\pi/2$. The other parameters are $\gamma_a = \gamma_b = \Gamma/100$, $\gamma_c = 100\Gamma$, $\Omega_{ab} = \Gamma/2$, $\Omega_{ca} = \Omega_{cb} = 5\Gamma$, and $\Delta_{cb} = \Delta_{ca} = \Delta_{ab} = 0$.

($|d\rangle$) or (b) different lower levels ($|d_1\rangle$, $|d_2\rangle$, and $|d_3\rangle$). The black solid curves are for phase $\Phi = \pi/2$ and the red dashed curves for $\Phi = 3\pi/2$. As expected for the spectra in both Figs. 3(a) and 3(b), there is a peak at the transition frequency ω_{ad} when $\Phi = 3\pi/2$ or a dip when $\Phi = \pi/2$. Comparing the curves of Figs. 3(a) and 3(b), we find that there is another dip around $\delta_k/\Gamma = -6.7$ in the spectrum of the system with one common lower level when $\Phi = \pi/2$, which is induced by destructive interference between different decay paths to one common lower level. As the dip around $\delta_k/\Gamma = -6.7$ is not induced by the nonreciprocal transitions, we do not explore it in the following.

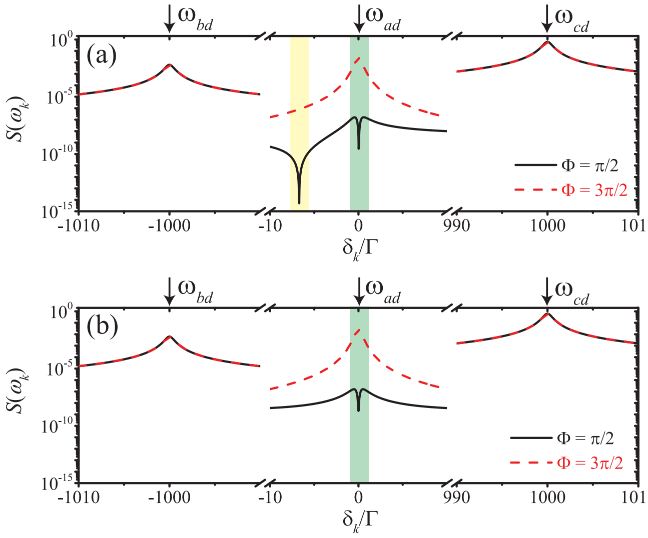

FIG. 3. Spontaneous emission spectra for the three upper levels ($|a\rangle$, $|b\rangle$, and $|c\rangle$) coupled by the same vacuum modes to (a) the common lower level ($|d\rangle$) or (b) different lower levels ($|d_1\rangle$, $|d_2\rangle$, and $|d_3\rangle$). The system is initially in level $|b\rangle$. The black solid curves are for phase $\Phi = \pi/2$ and the red dashed curves for $\Phi = 3\pi/2$. The other parameters are $\gamma_a = \gamma_b = \Gamma/100$, $\gamma_c = 100\Gamma$, $\Omega_{ab} = \Gamma/2$, $\Omega_{ca} = \Omega_{cb} = 5\Gamma$, $\Delta_{cb} = \Delta_{ca} = \Delta_{ab} = 0$, and $\omega_{ab} = \omega_{ca} = 10^3\Gamma$.

IV. SPONTANEOUS EMISSION SPECTRA OF CHIRAL MOLECULES

As an important application, we will discuss how to realize the determination of enantiomeric excess based on the spectral-line elimination in the spontaneous emission spectra of chiral molecules. Our method is based on the model of chiral molecules with cyclic-transition three upper levels coupled with one common lower level by the same vacuum modes, as shown in Fig. 4, where $|a\rangle_Q$, $|b\rangle_Q$, $|c\rangle_Q$, and $|d\rangle_Q$ ($Q = L, R$) are the inner states of the left- and right-handed molecules. Both the models of left- and right-handed molecules can be

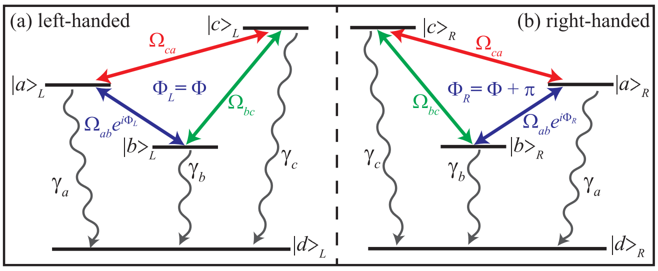

FIG. 4. Level diagram of a chiral molecule with cyclic transitions for the three upper levels ($|a\rangle_Q$, $|b\rangle_Q$, and $|c\rangle_Q$), and they are coupled by the same vacuum modes to the common lower level ($|d\rangle_Q$): (a) $Q = L$ for left-handed chiral states and (b) $Q = R$ for right-handed chiral states.

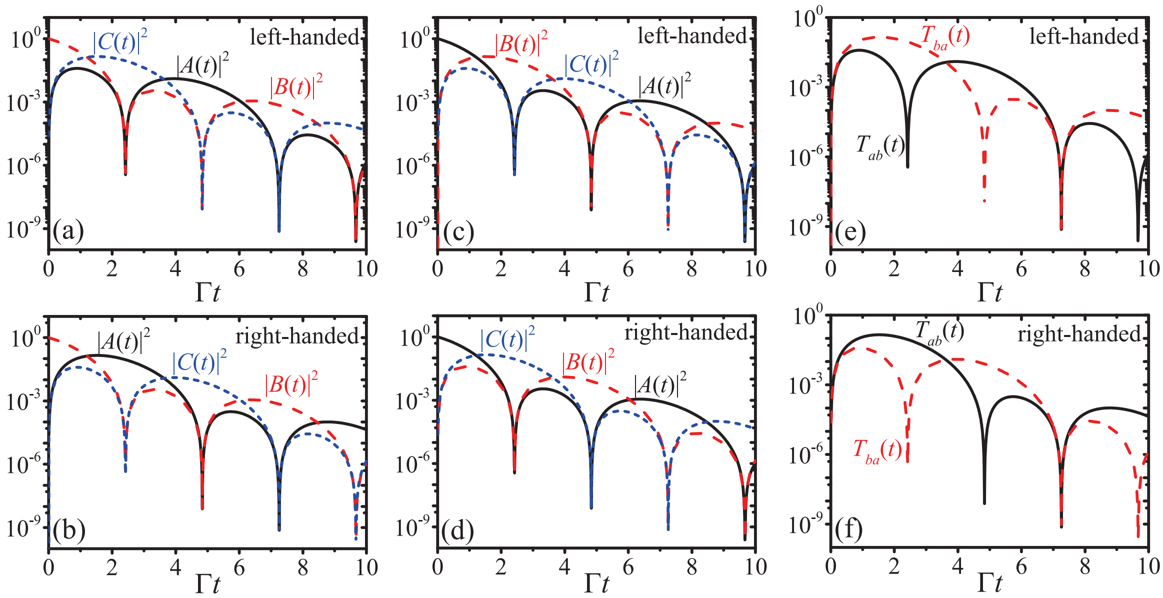

FIG. 5. Populations $|A(t)|^2$ (black solid curve), $|B(t)|^2$ (red dashed curve), and $|C(t)|^2$ (blue dot curve) are plotted as functions of the time Γt for left-handed molecules in (a) and (c) and right-handed molecules in (b) and (d). The initial conditions are $A(0) = C(0) = 0$ and $B(0) = 1$ for (a) and (b) and $B(0) = C(0) = 0$ and $A(0) = 1$ for (c) and (d). The transition probabilities $T_{ab}(t)$ and $T_{ba}(t)$ are plotted as functions of the time Γt for (e) left-handed molecules and (f) right-handed molecules. The other parameters are $\gamma_a = \gamma_b = \gamma_c = \Gamma$, $\Omega_{ab} = \Omega_{ca} = \Omega_{cb} = \Gamma/2$, $\Delta_{cb} = \Delta_{ca} = \Delta_{ab} = 0$, and $\Phi = \pi/2$.

described by the Hamiltonian given in Eq. (1) with $\Phi = \Phi_L$ for left-handed molecules and $\Phi = \Phi_R - \pi$ for right-handed molecules.

Let the chiral molecule initially be prepared in one of the upper levels $|a\rangle_Q$ and $|b\rangle_Q$. The time evolution of the populations in the three upper levels is shown in Figs. 5(a)–5(d). For the left-handed molecule, as shown in Fig. 5(a) with the molecule initially prepared in level $|b\rangle_L$, the population is transferred from $|b\rangle_L$ to $|c\rangle_L$ first, then to $|a\rangle_L$, and last back to $|b\rangle_L$, with the maximum population decaying exponentially; if the left-handed molecule is initially prepared in level $|a\rangle_L$ as shown in Fig. 5(c), the population is transferred from $|a\rangle_L$ to $|b\rangle_L$ first, then to $|c\rangle_L$, and last back to $|a\rangle_L$. In contrast, for the right-handed molecule, the population is transferred in the order $|b\rangle_R \to |a\rangle_R \to |c\rangle_R \to |b\rangle_R$ with the molecule initially prepared in level $|b\rangle_R$ as shown in Fig. 5(b), or in the order $|a\rangle_R \to |c\rangle_R \to |b\rangle_R \to |a\rangle_R$ with the molecule initially prepared in level $|a\rangle_R$ as shown in Fig. 5(d).

The chirality-dependent population transfer can be used for inner-state enantio separation [36–43,53]. We note that the similar cyclic transitions between three levels have been observed in a ring with three transmon superconducting qubits [58] and a single spin under closed-contour interaction [59]. Nevertheless, the exponential decay of the maximum population is one ingredient for nonreciprocal transition between the three upper levels, and the direction of the transition is chirality dependent. In Figs. 5(e) and 5(f), the transition probabilities $T_{ab}(t)$ and $T_{ba}(t)$ are plotted as functions of the time t for $\Phi = \pi/2$. The nonreciprocity is dynamical, i.e., sometimes the transition probability of $|a\rangle_Q$ to $|b\rangle_Q$ is greater than the one of $|b\rangle_Q$ to $|a\rangle_Q$ and sometimes the transition probability of $|b\rangle_Q$ to $|a\rangle_Q$ is greater than the one of $|a\rangle_Q$ to $|b\rangle_Q$. However, on average, the probability for the transition from $|a\rangle_L$ to $|b\rangle_L$ is greater than that from $|b\rangle_L$ to $|a\rangle_L$ in left-handed molecules and the probability for the transition from $|b\rangle_R$ to $|a\rangle_R$ is greater than that from $|a\rangle_R$ to $|b\rangle_R$ in right-handed molecules.

The nonreciprocal transition in the chiral molecules can be reflected in the spontaneous emission spectra. The spontaneous emission spectra for chiral molecules are plotted as a function of detuning δ_k in Fig. 6(a) with the black solid curves for left-handed molecules and the red dashed curves for right-handed molecules when $\Phi = \pi/2$. The most obvious difference between the two curves is there is one peak (with value S_L) at transition frequency ω_{cd} for left-handed molecules, but the peak is eliminated and a dip appears for right-handed molecules. By contrast, there is one peak (with value S_R) at transition frequency ω_{ad} for right-handed molecules, but the peak is eliminated for left-handed molecules. Then, the strengths of the spontaneous emission spectra of a chiral mixture, $S_M(\omega)$, at frequencies ω_{cd} and ω_{ad} are proportional to the molecule numbers of the two enantiomers, respectively,

$$S_M(\omega_{cd}) \approx N_L S_L, \tag{24}$$

$$S_M(\omega_{ad}) \approx N_R S_R, \tag{25}$$

where N_L (N_R) is the number of left-handed (right-handed) molecules. For the enantiomeric excess of a chiral mixture defined by $\varepsilon \equiv (N_L - N_R)/(N_L + N_R)$, the enantiomeric excess can be determined by

$$\varepsilon = \frac{S_M(\omega_{cd}) - \eta S_M(\omega_{ad})}{S_M(\omega_{cd}) + \eta S_M(\omega_{ad})}, \tag{26}$$

with the coefficient $\eta \equiv S_L/S_R$. Here, we have $\eta \approx 1$ with the parameters used in Figs. 5 and 6. In addition, the spontaneous emission spectra for chiral molecules show a sinusoidal dependence on the phase Φ, as shown in Fig. 6(b). $\Phi = \pi/2$ and

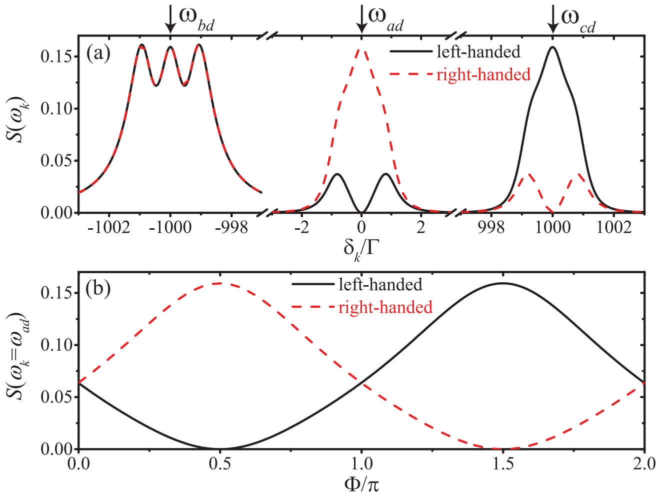

FIG. 6. Spontaneous emission spectra for a (left-handed or right-handed) chiral molecule with three upper levels ($|a\rangle_Q$, $|b\rangle_Q$, and $|c\rangle_Q$) coupled by the same vacuum modes to a common lower level ($|d\rangle_Q$). The molecule is initially in level $|b\rangle_Q$. The black solid curves are for the ($Q = L$) left-handed molecule and the red dashed curves for the ($Q = R$) right-handed molecule. (a) The spontaneous emission spectra versus δ_k for $\Phi = \pi/2$; (b) the spontaneous emission spectra versus Φ for $\omega_k = \omega_{ad}$. The other parameters are $\gamma_a = \gamma_b = \gamma_c = \Gamma$, $\Omega_{ab} = \Omega_{ca} = \Omega_{cb} = \Gamma/2$, $\Delta_{cb} = \Delta_{ca} = \Delta_{ab} = 0$, and $\omega_{ab} = \omega_{ca} = 10^3\Gamma$.

$\Phi = 3\pi/2$ are two optimal phases to make the determination of enantiomeric excess mostly efficiently.

V. CONCLUSIONS

In conclusion, we have studied the spontaneous emission spectrum of a multilevel system with nonreciprocal transition. Spectral line elimination appears in the spectra when there is almost no population transferring in one of the transition directions for nonreciprocal transition. To observe these phenomena, it is most important to realize cyclic three-level transition by breaking the symmetry of the potential of the emitters. The cyclic three-level transition has been proposed and observed in the superconducting qubit circuit with three Josephson junctions [19,60], a single nitrogen-vacancy center embedded in a mechanical resonator [59], and also the chiral molecules [22–33] .

As an important application, the spectral-line elimination induced by nonreciprocal transition provides us a method to determine the enantiomeric excess for the chiral molecules without requiring the enantio-pure samples. When the spectral-line elimination appears at some resonant frequencies for molecules with one chirality, the strengths of the spontaneous emission spectra at those frequencies are proportional to the numbers of the molecules with the opposite chirality, so the enantiomeric excess can be determined by measuring the strengths of the spontaneous emission spectra at these frequencies. The model of the chiral molecules for determining the enantiomeric excess is general and the method may be used to distinguish the enantiomers of 1,2-propanediol [23], 1,3-butanediol [24], and 4-carvomenthenol [29].

In order to realize these in experiments, some more problems should be considered. To obtain real single-loop three-level configuration with no connections to other states, the tops of the chiral molecules should be asymmetric [20,32]. If the real single-loop cyclic three-level subsystem is constructed with rotational transitions, the wave vectors of the three driving fields cannot be parallel [20], thus leading to inevitable phase mismatching.

In order to ensure all molecules are approximately in phase, the characteristic length of the medium should be much smaller than the largest wavelength of the three driving fields [2,39]. In practice, two of the three states $|a\rangle$, $|b\rangle$, and $|c\rangle$ can be chosen in the same vibrational excited state. Then, they are coupled with a microwave field. In this way, it is easier to make the molecules approximately phase matched than the case that the three states are in three different vibrational states.

Moreover, to achieve enantiomeric-excess determination, the three states in the cyclic three-level model can have different vibrational sublevels so that the energy spacings of them may be large enough to assume all population starting in one state. If the three states in the cyclic three-level model have the same vibrational sublevel, in order to assume all population starting in one state, the rotational temperature should be cooled sufficiently initially [30], such that there is almost no population in the upper states before one upper state being populated by selective pumping.

In addition, the Purcell effect [61] is an important phenomenon in spontaneous emission and may enhance the predicted effects in this work.

ACKNOWLEDGMENTS

X.-W.X. is supported by the National Natural Science Foundation of China (NSFC) under Grant No. 11604096, and the Key Program of Natural Science Foundation of Jiangxi Province, China under Grant No. 20192ACB21002. C.Y. is supported by NSFC under Grant No. 11947206. Y.L. is supported by National Key R&D Program of China under Grant No. 2016YFA0301200, and NSFC under Grants No. 11774024 and No. U1930402. A.-X.C. is supported by NSFC under Grant No. 11775190.

APPENDIX: DERIVATION OF THE TRANSITION PROBABILITIES

The dynamic equations (10)–(12) can be concisely expressed as

$$i\frac{d\Psi(t)}{dt} = H_{\text{eff}}\Psi(t), \tag{A1}$$

where $\Psi(t) = [A(t), \widetilde{B}(t), \widetilde{C}(t)]^{\mathsf{T}}$, and

$$H_{\text{eff}} = \begin{pmatrix} -i\frac{\gamma_a}{2} & \Omega_{ab}e^{i\Phi} & \Omega_{ca} \\ \Omega_{ab}e^{-i\Phi} & -\Delta_{ab} - i\frac{\gamma_b}{2} & \Omega_{cb} \\ \Omega_{ca} & \Omega_{cb} & \Delta_{ca} - i\frac{\gamma_c}{2} \end{pmatrix}. \tag{A2}$$

Then we have

$$\Psi(t) = U(t)\Psi(0), \tag{A3}$$

with the initial conditions $\Psi(0) = [A(0), B(0), C(0)]^{\intercal}$, and the time-evolution matrix

$$U(t) \equiv e^{-iH_{\text{eff}}t}. \tag{A4}$$

The transition probabilities from $|a\rangle$ to $|b\rangle$ $[T_{ba}(t)]$ and from $|b\rangle$ to $|a\rangle$ $[T_{ab}(t)]$ are defined as

$$T_{ba}(t) \equiv |U_{21}(t)|^2, \tag{A5}$$

$$T_{ab}(t) \equiv |U_{12}(t)|^2, \tag{A6}$$

where $U_{ij}(t)$ (for $i, j = 1, 2, 3$) represents the element at the ith row and jth column of the matrix $U(t)$ given by Eq. (A4).

[1] D. Jalas, A. Petrov, M. Eich, W. Freude, S. Fan, Z. Yu, R. Baets, M. Popović, A. Melloni, J. D. Joannopoulos, M. Vanwolleghem, C. R. Doerr, and H. Renner, What is - and what is not - an optical isolator, Nat. Photon. **7**, 579 (2013).

[2] C. Caloz, A. Alù, S. Tretyakov, D. Sounas, K. Achouri, and Z.-L. Deck-Léger, Electromagnetic Nonreciprocity, Phys. Rev. Appl. **10**, 047001 (2018).

[3] A. A. Mazneva, A. G. Every, and O. B. Wright, Reciprocity in reflection and transmission: What is a ‘phonon diode’? Wave Motion **50**, 776 (2013).

[4] R. Fleury, D. L. Sounas, C. F. Sieck, M. R. Haberman, and A. Alù, Sound isolation and giant linear nonreciprocity in a compact acoustic circulator, Science **343**, 516 (2014).

[5] M. Atala, M. Aidelsburger, M. Lohse, J. T. Barreiro, B. Paredes, and I. Bloch, Observation of chiral currents with ultracold atoms in bosonic ladders, Nat. Phys. **10**, 588 (2014).

[6] X. W. Xu, Y. J. Zhao, H. Wang, A. X. Chen, and Y. X. Liu, Nonreciprocal transition between two nondegenerate energy levels, arXiv:1908.08323.

[7] J. Zhang, B. Peng, S. K. Özdemir, Y. X. Liu, H. Jing, X. Y. Lü, Y. L. Liu, L. Yang, and F. Nori, Giant nonlinearity via breaking parity-time symmetry: A route to low-threshold phonon diodes, Phys. Rev. B **92**, 115407 (2015).

[8] Y. Jiang, S. Maayani, T. Carmon, F. Nori, and H. Jing, Nonreciprocal Phonon Laser, Phys. Rev. Appl. **10**, 064037 (2018).

[9] A. I. Lvovsky, B. C. Sanders, and W. Tittel, Optical quantum memory, Nat. Photon. **3**, 706 (2009).

[10] A. A. Clerk, M. H. Devoret, S. M. Girvin, F. Marquardt, and R. J. Schoelkopf, Introduction to quantum noise, measurement, and amplification, Rev. Mod. Phys. **82**, 1155 (2010).

[11] S. Y. Zhu, R. C. F. Chan, and C. P. Lee, Spontaneous emission from a three-level atom, Phys. Rev. A **52**, 710 (1995).

[12] S. Y. Zhu and M. O. Scully, Spectral Line Elimination and Spontaneous Emission Cancellation via Quantum Interference, Phys. Rev. Lett. **76**, 388 (1996).

[13] *Chiral Analysis*, edited by K. W. Busch and M. A. Busch (Elsevier, Amsterdam, 2006).

[14] P. J. Stephens, Theory of vibrational circular dichroism, J. Phys. Chem. **89**, 748 (1985).

[15] M. M. R. Fanood, N. B. Ram, C. S. Lehmann, I. Powis, and M. H. M. Janssen, Enantiomer-specific analysis of multi-component mixtures by correlated electron imaging–ion mass spectrometry, Nat. Commun. **6**, 7511 (2015).

[16] Y. He, B. Wang, R. K. Dukor, and L. A. Nafie, Determination of absolute configuration of chiral molecules using vibrational optical activity: A review, Appl. Spectrosc. **65**, 699 (2011).

[17] T. Kh. Begzjav, Z. Zhang, M. O. Scully, and G. S. Agarwal, Enhanced signals from chiral molecules via molecular coherence, Opt. Express **27**, 13965 (2019).

[18] N. A. Ansari, J. Gea-Banacloche, and M. S. Zubairy, Phase-sensitive amplification in a three-level atomic system, Phys. Rev. A **41**, 5179 (1990).

[19] Y. X. Liu, J. Q. You, L. F. Wei, C. P. Sun, and F. Nori, Optical Selection Rules and Phase-Dependent Adiabatic State Control in a Superconducting Quantum Circuit, Phys. Rev. Lett. **95**, 087001 (2005).

[20] C. Ye, Q. Zhang, and Y. Li, Real single-loop cyclic three-level configuration of chiral molecules, Phys. Rev. A **98**, 063401 (2018).

[21] W. Z. Jia and L. F. Wei, Probing molecular chirality by coherent optical absorption spectra, Phys. Rev. A **84**, 053849 (2011).

[22] E. Hirota, Triple resonance for a three-level system of a chiral molecule, Proc. Jpn. Acad., Ser. B **88**, 120 (2012).

[23] D. Patterson, M. Schnell, and J. M. Doyle, Enantiomer-specific detection of chiral molecules via microwave spectroscopy, Nature (London) **497**, 475 (2013).

[24] D. Patterson and J. M. Doyle, Sensitive Chiral Analysis via Microwave Three-Wave Mixing, Phys. Rev. Lett. **111**, 023008 (2013).

[25] D. Patterson and M. Schnell, New studies on molecular chirality in the gas phase: Enantiomer differentiation and determination of enantiomeric excess, Phys. Chem. Chem. Phys. **16**, 11114 (2014).

[26] V. A. Shubert, D. Schmitz, D. Patterson, J. M. Doyle, and M. Schnell, Identifying enantiomers in mixtures of chiral molecules with broadband microwave spectroscopy, Angew. Chem. Int. Ed. **53**, 1152 (2014).

[27] S. Lobsiger, C. Pérez, L. Evangelisti, K. K. Lehmann, and B. H. Pate, Molecular structure and chirality detection by Fourier transform microwave spectroscopy, J. Phys. Chem. Lett. **6**, 196 (2015).

[28] V. A. Shubert, D. Schmitz, C. Pérez, C. Medcraft, A. Krin, S. R. Domingos, D. Patterson, and M. Schnell, Chiral analysis using broadband rotational spectroscopy, J. Phys. Chem. Lett. **7**, 341 (2015).

[29] V. A. Shubert, D. Schmitz, C. Medcraft, A. Krin, D. Patterson, J. M. Doyle, and M. Schnell, Rotational spectroscopy and three-wave mixing of 4-carvomenthenol: A technical guide to measuring chirality in the microwave regime, J. Chem. Phys. **142**, 214201 (2015).

[30] S. Eibenberger, J. M. Doyle, and D. Patterson, Enantiomer-Specific State Transfer of Chiral Molecules, Phys. Rev. Lett. **118**, 123002 (2017).

[31] C. Perez, A. L. Steber, S. R. Domingos, A. Krin, D. Schmitz, and M. Schnell, Coherent enantiomer-selective population enrichment using tailored microwave fields, Angew. Chem. Int. Ed. **56**, 12512 (2017).

[32] M. Leibscher, T. F. Giesen, and C. P. Koch, Principles of enantio-selective excitation in three-wave mixing spectroscopy of chiral molecules, J. Chem. Phys. **151**, 014302 (2019).

[33] C. P. Koch, M. Lemeshko, and D. Sugny, Quantum control of molecular rotation, Rev. Mod. Phys. **91**, 035005 (2019).

[34] C. Ye, Q. Zhang, Y. Y. Chen, and Y. Li, Determination of enantiomeric excess with chirality-dependent ac Stark effects in cyclic three-level models, Phys. Rev. A **100**, 033411 (2019).

[35] Y. Y. Chen, C. Ye, Q. Zhang, and Y. Li, Enantio-discrimination via light deflection effect, J. Chem. Phys. **152**, 204305 (2020).

[36] P. Král and M. Shapiro, Cyclic Population Transfer in Quantum Systems with Broken Symmetry, Phys. Rev. Lett. **87**, 183002 (2001).

[37] Y. Li and C. Bruder, Dynamic method to distinguish between left- and right-handed chiral molecules, Phys. Rev. A **77**, 015403 (2008).

[38] W. Z. Jia and L. F. Wei, Distinguishing left- and right-handed molecules using two-step coherent pulses, J. Phys. B: At., Mol., Opt. Phys. **43**, 185402 (2010).

[39] K. K. Lehmann, Influence of spatial degeneracy on rotational spectroscopy: Three-wave mixing and enantiomeric state separation of chiral molecules, J. Chem. Phys. **149**, 094201 (2018).

[40] N. V. Vitanov and M. Drewsen, Highly Efficient Detection and Separation of Chiral Molecules through Shortcuts to Adiabaticity, Phys. Rev. Lett. **122**, 173202 (2019).

[41] C. Ye, Q. Zhang, and Y. Li, Static nonlinear Schrödinger equations for the achiral-chiral transitions of polar chiral molecules, Phys. Rev. A **99**, 062703 (2019).

[42] C. Ye, Q. Zhang, Y. Y. Chen, and Y. Li, Effective two-level models for highly efficient inner-state enantio-separation based on cyclic three-level systems of chiral molecules, Phys. Rev. A **100**, 043403 (2019).

[43] J. L. Wu, Y. Wang, J. Song, Y. Xia, S. L. Su, and Y. Y. Jiang, Robust and highly efficient discrimination of chiral molecules through three-mode parallel paths, Phys. Rev. A **100**, 043413 (2019).

[44] Y. Li, C. Bruder, and C. P. Sun, Generalized Stern-Gerlach Effect for Chiral Molecules, Phys. Rev. Lett. **99**, 130403 (2007).

[45] X. Li and M. Shapiro, Theory of the optical spatial separation of racemic mixtures of chiral molecules, J. Chem. Phys. **132**, 194315 (2010).

[46] A. Jacob and K. Hornberger, Effect of molecular rotation on enantioseparation, J. Chem. Phys. **137**, 044313 (2012).

[47] C. Brand, B. A. Stickler, C. Knobloch, A. Shayeghi, K. Hornberger, and M. Arndt, Conformer Selection by Matter-Wave Interference, Phys. Rev. Lett. **121**, 173002 (2018).

[48] A. A. Milner, J. A. M. Fordyce, I. MacPhail-Bartley, W. Wasserman, V. Milner, I. Tutunnikov, and I. Sh. Averbukh, Controlled Enantioselective Orientation of Chiral Molecules with an Optical Centrifuge, Phys. Rev. Lett. **122**, 223201 (2019).

[49] F. Suzuki, T. Momose, and S. Y. Buhmann, Stern-Gerlach separator of chiral enantiomers based on the Casimir-Polder potential, Phys. Rev. A **99**, 012513 (2019).

[50] M. Shapiro, E. Frishman, and P. Brumer, Coherently Controlled Asymmetric Synthesis with Achiral Light, Phys. Rev. Lett. **84**, 1669 (2000).

[51] P. Brumer, E. Frishman, and M. Shapiro, Principles of electric-dipole-allowed optical control of molecular chirality, Phys. Rev. A **65**, 015401 (2001).

[52] D. Gerbasi, M. Shapiro, and P. Brumer, Theory of enantiomeric control in dimethylallene using achiral light, J. Chem. Phys. **115**, 5349 (2001).

[53] P. Král, I. Thanopulos, M. Shapiro, and D. Cohen, Two-Step Enantio-Selective Optical Switch, Phys. Rev. Lett. **90**, 033001 (2003).

[54] E. Frishman, M. Shapiro, and P. Brumer, Optical purification of racemic mixtures by 'laser distillation' in the presence of a dissipative bath, J. Phys. B: At., Mol., Opt. Phys. **37**, 2811 (2004).

[55] C. Ye, Q. Zhang, Y. Y. Chen, and Y. Li, Fast enantioconversion of chiral mixtures based on a four-level double-Δ model, Phys. Rev. Research **2**, 033064 (2020).

[56] V. Weisskopf and E. Wigner, Berechnung der natürlichen linienbreite auf grund der diracschen lichttheorie, Z. Phys. **63**, 54 (1930).

[57] M. O. Scully and M. S. Zubairy, *Quantum Optics* (Cambridge University Press, Cambridge, England, 1997).

[58] P. Roushan, C. Neill, A. Megrant, Y. Chen, R. Babbush, R. Barends, B. Campbell, Z. Chen, B. Chiaro, A. Dunsworth, A. Fowler, E. Jeffrey, J. Kelly, E. Lucero, J. Mutus, P. J. J. O'Malley, M. Neeley, C. Quintana, D. Sank, A. Vainsencher, J. Wenner, T. White, E. Kapit, H. Neven, and J. Martinis, Chiral ground-state currents of interacting photons in a synthetic magnetic field, Nat. Phys. **13**, 146 (2017).

[59] A. Barfuss, J. Kölbl, L. Thiel, J. Teissier, M. Kasperczyk, and P. Maletinsky, Phase-controlled coherent dynamics of a single spin under closed-contour interaction, Nat. Phys. **14**, 1087 (2018).

[60] J. E. Mooij, T. P. Orlando, L. Levitov, L. Tian, C. H. van der Wal, and S. Lloyd, Josephson persistent-current qubit, Science **285**, 1036 (1999).

[61] E. M. Purcell, Spontaneous emission probabilities at radio frequencies, Phys. Rev. **69**, 681 (1946).